A&A 432, 567–574 (2005)
DOI: 10.1051/0004-6361:20041402

Astronomy & Astrophysics

3-D kinematics of the HH 110 jet⋆

R. López[1], R. Estalella[1], A. C. Raga[2], A. Riera[3,1], B. Reipurth[4], and S. R. Heathcote[5]

[1] Departament d'Astronomia i Meteorologia, Universitat de Barcelona, Av. Diagonal 647, 08028 Barcelona, Spain
e-mail: [rosario;robert.estalella]@am.ub.es
[2] Instituto de Ciencias Nucleares, Universidad Nacional Autónoma de México, Apartado Postal 70-543, 04510 México D.F., México
e-mail: raga@nuclecu.unam.mx
[3] Departament de Física i Enginyeria Nuclear, Universitat Politècnica de Catalunya, Av. Víctor Balaguer s/n, 08800 Vilanova i la Geltrú, Spain
e-mail: angels.riera@upc.es
[4] Institute for Astronomy, University of Hawaii, 2680 Woodlawn Drive, Honolulu, HI 96822, USA
e-mail: reipurth@ifa.hawaii.edu
[5] Southern Astrophysical Research Telescope, Casilla 603, La Serena, Chile
e-mail: sheathcote@ctio.noao.edu

Received 3 June 2004 / Accepted 8 November 2004

Abstract. We present new results on the kinematics of the jet HH 110. New proper motion measurements have been calculated from [SII] CCD images obtained with a time baseline of nearly fifteen years. HH 110 proper motions show a strong asymmetry with respect to the outflow axis, with a general trend of pointing towards the west of the axis direction. Spatial velocities have been obtained by combining the proper motions and radial velocities from Fabry-Pérot data. Velocities decrease by a factor ∼3 over a distance of $\sim 10^{18}$ cm, much shorter than the distances expected for the braking caused by the jet/environment interaction. Our results show evidence of an anomalously strong interaction between the outflow and the surrounding environment, and are compatible with the scenario in which HH 110 emerges from a deflection in a jet/cloud collision.

Key words. ISM: individual: HH 110 – ISM: jets and outflows – stars: pre-main sequence – ISM: Herbig-Haro objects

1. Introduction

The HH 110 jet (which is found in the Orion B cloud complex) was discovered by Reipurth & Olberg (1991). This jet presents a morphology in Hα and [SII] images that is quite different from the morphologies of other well known stellar jets. While the best studied jets (e.g., HH 111 and HH 34) show chains of aligned knots with more or less organized, arc-like shapes, the HH 110 jet has a more chaotic structure: it starts in a well collimated chain of knots and then widens in a cone of opening angle ∼10°, with a rather chaotic knot structure and appreciable wiggles along the length of the jet. The observed structure is reminiscent of a turbulent outflow.

In contrast to the optical images, the HH 110 jet is nearly straight in near infrared H_2 2.12 μm images. Furthermore, the H_2 emission appears shifted westward relative to the optical emission (Noriega-Crespo et al. 1996).

Another special feature of the HH 110 jet is the lack of detection of any stellar source (suitable for powering the jet) along the outflow axis. The morphology of HH 110 first suggested that the driving jet source would be embedded in a dark lane located to the north of the apex of the outflow. However, searches at optical, near infrared and radio continuum wavelengths have failed to detect the HH 110 driving source.

Reipurth et al. (1996) report the discovery of another fainter jet, HH 270, located 3′ northeast of HH 110. An embedded near-infrared source very close to IRAS 05489+0256 was also found along the HH 270 flow axis. They suggest that HH 110 is the result of the deflection of the HH 270 jet (which travels in an E-W direction) through a collision with a dense molecular cloud core. In this scenario, HH 270 strikes the molecular core and is deflected, giving rise to the HH 110 jet. The H_2 emission would then be a tracer of the region where the atomic jet and the molecular cloud core interact (Noriega-Crespo et al. 1996).

Because of the interesting dynamics resulting from the interaction between a radiative jet and a dense obstacle, a number of theoretical papers on the HH 270/HH 110 system have been written. Cantó & Raga (1996) explored the initial stages of a jet/cloud collision with both analytic models and time-dependent, 2D numerical simulations. The final, steady state in which the jet has bored a hole through the (stratified)

⋆ Partially based on observations made with the 2.5 m Isaac Newton and the Nordic Optical Telescopes operated at the Observatorio del Roque de los Muchachos of the Instituto de Astrofísica de Canarias.

Table 1. Log of the data.

Epoch	Telescope	Pixel scale (arcsec)	Exp. time (s)	Reference
1987 Dec. 18	1.5 m La Silla	0.35	3600	1
1988 Mar. 5	3.6 m ESO	0.35	1800	1
1993 Dec. 16	2.5 m INT	0.55	9000	2
1994 Jan. 15	3.5 m NTT	0.35	1200	1
2002 Oct. 24	2.6 m NOT	0.19	9000	3

References: (1) Reipurth et al. (1996); (2) Riera et al. (2003a); (3) obtained by G. Gómez through the NOT Service Time facility.

cloud was studied analytically and numerically by Cantó & Raga (1996) and Raga & Cantó (1996). The initial state of a jet/cloud interaction (which we now appear to be seeing in the HH 270/HH 110 system) was re-explored, now with 3D numerical simulations, by de Gouveia dal Pino (1999). Hurka et al. (1999) carried out 3D numerical simulations of a jet interacting with a magnetized cloud. The most recent paper on models of a radiative jet/dense cloud interaction is the one of Raga et al. (2002), who carried out 3D simulations with a simplified atomic/molecular network in order to obtain predictions of atomic and molecular emission line maps for carrying out direct comparisons with the HH 270/HH 110 system.

The HH 110 jet seems to be appropriate for searching the observational signatures of entrainment and turbulence through spatially resolved kinematic studies. Recently, Riera et al. (2003a,b) presented detailed radial velocity studies obtained with multi-long-slit spectroscopy and Fabry-Pérot interferometry, and compared the observations with simple, parametrized models of a turbulent jet (Cantó et al. 2003).

In order to complement these radial velocity studies, we now present new proper motion measurements of HH 110. These proper motions have been determined from deep [SII] CCD images that were obtained with a time baseline of 5424 days (i.e., nearly fifteen years), and show the kinematical properties of a large number of knots. The only previous proper motion determinations of HH 110 are those of Reipurth et al. (1996), who study images with a shorter time baseline (~6 yr) and are not able to reach a level of accuracy and detail comparable to that of our present measurements.

The paper is organized as follows. The observations are described in Sect. 2. In Sect. 3 we present the procedures to measure the proper motion velocities (Sect. 3.1) and discuss the obtained results (Sect. 3.2). The radial and total velocities are discussed in Sect. 4. Finally, the conclusions are given in Sect. 5.

2. Observations

In order to determine proper motions of HH 110 jet, a set of five CCD images has been used, yielding a time baseline of 5424 days (nearly fifteen years). Details of the epochs, telescopes, spatial resolution and exposure times are given in Table 1. All the images were obtained through [SII] narrow-band filters, which included the [SII] $\lambda = 6717, 6731$ Å emission lines. It is not possible to perform similar proper motion determinations from the Hα emission, as we did not obtain images through an Hα narrow-band filter during the observing runs carried out in the 1993 and 2002 epochs.

The 1987 image was obtained at the Danish 1.5 m Telescope at La Silla. The 1988 image was obtained at the ESO 3.6 m Telescope. The 1994 image was obtained with EMMI at the ESO 3.5 m New Technology Telescope (NTT). Details on the acquisition and treatment of all these data can be found in the papers of Reipurth & Olberg (1991) and Reipurth et al. (1996).

The 1993 image was obtained at the prime focus of the 2.5-m Isaac Newton Telescope (INT) of the Observatorio del Roque de los Muchachos (ORM, La Palma, Spain). The detector used was a CCD with a coated EEV chip. A filter of central wavelength $\lambda = 6730$ Å and bandpass $\Delta\lambda = 48$ Å was used.

The 2002 image was obtained with the 2.6-m Nordic Optical Telescope (NOT) of the ORM. The Andalucia Faint Object Spectrograph and Camera (ALFOSC) was used, with a Ford-Loral CCD, and a filter of central wavelength $\lambda = 6724$ Å and bandpass $\Delta\lambda = 50$ Å. Both the 1993 and the 2002 images were obtained by combining five frames of 1800 s exposure each. For these two epochs, the individual exposures were reduced (bias-subtracted and flat-fielded) using the same procedure, through the standard tasks of the IRAF[1] reduction package. The five individual frames were recentered using the position of several field stars, in order to correct for misalignments among the individual frames. Then the frames were median-averaged using the IMCOMBINE task of IRAF (with appropriate options to remove cosmic ray events). We obtained one deep [SII] image with a total integration time of 2.5 h for each of these two epochs (i.e., 1993 and 2002). These final images are not flux-calibrated.

The central radial velocities of the main knots of HH 110 were obtained from Hα Fabry-Pérot data (see Riera et al. 2003b for more details of the observations and the data reduction).

3. Proper motion measurements

3.1. Method and results

Proper motions of the main HH 110 knots have been determined from the CCD images listed in Table 1. First, the five images were converted onto a common reference system and

[1] IRAF is distributed by the National Optical Astronomy Observatories, which are operated by the Association of Universities for Reseach in Astronomy, Inc., under cooperative with the National Science Foundation.

rebinned to the same pixel scale. We used the position of fifteen common field stars, in order to register the images. These reference stars are well distributed around the HH 110 jet. The GEOMAP and GEOTRAN tasks of IRAF were applied to perform a linear transformation with six free parameters that take into account relative translation, rotation and magnifications between the frames. The final, transformed frames have a pixel size of 0.″35.

In order to check the accuracy obtained for the common reference system of the five final images, two tests were performed:

- Firstly, the displacements of the reference field stars in all images were calculated by computing the peak of the two-dimensional cross-correlation function between pairs of frames (i.e., the first-epoch, 1987, and each of the other images) over small boxes around the reference stars. The average and rms of the displacements for the four pairs of images were less than 0.09 ± 0.18 pixels for the x coordinate, and less than 0.04 ± 0.14 pixels for the y coordinate.
- Secondly, to test the accuracy of the transformations described above, we carried out astrometry for each of the final images, using the (α, δ) coordinates of five bright field stars obtained from the USNO-B1.0 Catalogue[2]. With this procedure we confirmed that the pixel size indeed corresponds to 0.″35 (see above) and that the orientation of each of the final images differs from the true North direction by less than 0.°4.

Thus, we concluded that the five final images used for the proper motion determinations were properly scaled and aligned, and were therefore suitable for estimating the proper motions of the HH 110 knots.

In order to calculate proper motions for the knots of HH 110, we first defined boxes in each frame that included the emission from the individual knots (see Table 2 and Fig. 1 for the nomenclature of the knots and the definition of the boxes). Then, for the four pairs of frames (i.e., the 1987 first epoch and each of the other images) we computed the two-dimensional cross-correlation function of the emission within the pairs of boxes, and we determined the displacement in the x and y coordinates through a parabolic fit to the peak of the cross-correlation function (see Reipurth et al. 1996; and López et al. 1996, for more details of this procedure). For each knot, the uncertainty in the position of the correlation peak was estimated through the scatter of the correlation peak positions corresponding to boxes shifted from the nominal box by 0 or ±2 pixels (i.e., 0.″7) on each of its four sides (giving a total of 3^4 different boxes for each knot). We adopted as error for each coordinate twice the rms deviation of the positions of the cross-correlation peaks, added quadratically to the rms alignment error.

The errors in the displacements obtained for the 1988 image were much greater than for the rest of the images. This is probably a consequence of the poor quality of the image. Thus, we decided to discard the data obtained from this image from the rest of the analysis and use only the displacements from the 1987 image to the images of 1993, 1994, and 2002.

[2] The USNOFS Image and Catalogue Archive is operated by the United States Naval Observatory, Flagstaff Station.

Table 2. HH 110 proper motions[a].

Knot	Offset[b] (arcsec)	V_T (km s^{-1})	PA (deg)	ΔPA[c] (deg)
A	0.0	181.9 ± 5.2	215 ± 2	21
B	7.9	24.2 ± 3.7	134 ± 9	−58
B′	14.9	25.6 ± 2.6	273 ± 6	79
C	22.8	163.0 ± 5.8	222 ± 2	28
E	40.1	75.4 ± 4.0	213 ± 3	19
H′	42.8	153.5 ± 7.6	206 ± 3	12
H	48.4	133.3 ± 3.9	220 ± 2	26
I_E	61.0	44.4 ± 2.0	197 ± 1	3
I_W	62.3	144.7 ± 22.3	230 ± 7	36
J_N	62.4	159.8 ± 17.8	186 ± 4	−8
J_S	70.0	157.0 ± 7.3	202 ± 2	8
L	73.0	119.0 ± 7.7	206 ± 6	12
M	81.3	106.6 ± 2.9	207 ± 3	13
N	91.9	148.1 ± 4.0	201 ± 4	7
O	101.8	183.7 ± 5.4	209 ± 2	15
P	113.6	91.5 ± 2.7	184 ± 4	−10
Q	121.2	104.1 ± 5.2	185 ± 1	−9
R	152.0	84.9 ± 24.8	128 ± 20	−66
S	179.1	68.9 ± 2.5	216 ± 2	22

[a] A distance of 460 pc has been adopted.
[b] Offset from knot A (at the 1987 epoch) along the jet outflow axis.
[c] ΔPA is defined as $PA_{pm} - PA_j$.

Finally, for each knot, we performed a linear regression fit to the displacements in each coordinate as a function of epoch offset from the first epoch (1987). For each coordinate of each knot we fitted a straight line to four points: a zero displacement for epoch offset zero, and the three measured displacements. The fit was performed taking into account the error associated with each displacement. We assigned to the zero displacement an error equal to the quadratic average error of the three measured displacements. The fits obtained for the (x, y) coordinates of the different knots are shown in Fig. 2. From the slope of the fitted straight line and its uncertainty we determined the proper motion velocity (V_T) and position angle (PA) of each knot and their uncertainties. These values are listed in Table 2 and displayed in Fig. 1. A distance to HH 110 of 460 pc has been adopted.

3.2. Discussion

Let us first define the HH 110 outflow axis passing through knots A to C, which define a well aligned structure. The outflow axis defined in this way has $PA_j = 193.°6$. From Fig. 1, it is clear that, as a general trend, the proper motion velocities show a small westward deviation relative to this axis. This westward deviation tends to diminish as one goes southwards from knot A. If one compares our Fig. 1 with Fig. 4 of Reipurth et al. (1996), one sees a general agreement between the two sets of results. However, there are substantial differences for some of the knots, which are discussed in detail below.

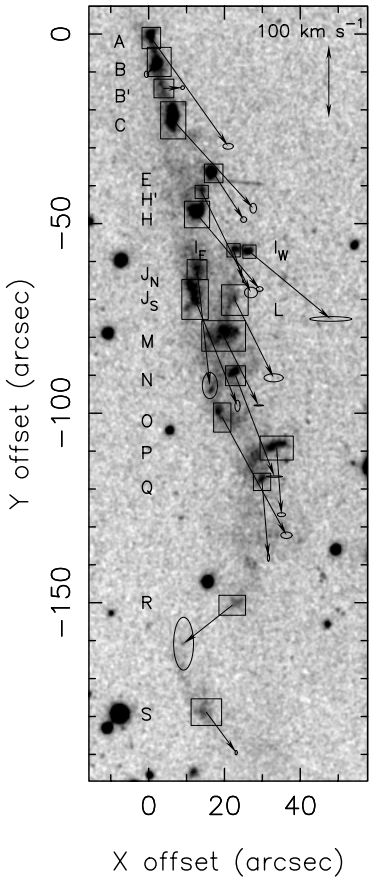

Fig. 1. [SII] 6717+6731 image of HH 110 from the October 2002 NOT image. Arrows indicate the proper motion velocity of each knot. Ellipses at the end of each arrow indicate the uncertainty in the components of the velocity vector. The scale of the arrows is indicated by the double headed arrow at the top right corner of the map, and corresponds to a velocity of 100 km s^{-1}. Boxes indicate the regions used for the proper motion calculations. Offsets are measured from the peak position of knot A. North is up and East is to the left.

At distances >130″ south from knot A the emitting knots show large deviations with respect to the outflow axis, with a locus that first curves to the E and then to the W, becoming again more or less parallel to the outflow axis. In this region, we have measured the proper motions of knot R (which is moving to the SE, in a direction parallel to the locus of the jet) and condensation S (again moving parallel to the locus of the jet, which in this position is also approximately parallel to the outflow axis). The resulting structure is quite striking, as it apparently shows that the knots are flowing along a curved "channel", in contrast to the expected behaviour of a pure ballistic motion (note that the knot proper motions are always parallel to the local direction of the locus of the emitting region). However, as can be seen from Fig. 1, this conclusion is mostly based on the SE proper motion of knot R, which has a highly uncertain measured proper motion. If we remove this knot from the analysis, we would only conclude that all of the knots of HH 110 have proper motions directed sligthly to the W of the outflow axis.

In order to illustrate the westward shift, we calculate the differences $\Delta PA = PA_{pm} - PA_j$ between the directions of the proper motions and the direction of the HH 110 axis, $PA_j = 193\overset{\circ}{.}6$ (see above). In Fig. 3 we plot these angular differences as a function of distance along the outflow axis. In this figure we see that knots P, Q and J_N move in a direction to the E of the HH 110 axis. Knot R also moves to the E (but, as we have discussed above, it is not clear whether or not this proper motion measurement is significant), and the remaining 13 knots with measured proper motions move in a direction to the W of the HH 110 axis. In this figure the corresponding directions of the HH 110 and HH 270 jet axes have been indicated by dashed (for HH 110) and dotted (for HH 270) lines, respectively. The directions of the motions of these 13 knots lie in between the HH 110 axis and the HH 270 axis (the jet that is apparently deflected through a collision in order to form HH 110). In addition, this plot shows that while for the knots with distances $d < 50''$ from knot A the proper motions have $PA_{pm} - PA_j \sim 10^\circ$ to 30° (with an average value $\langle PA_{pm} - PA_j \rangle = 21^\circ$), for distances $50'' < d < 130''$ the proper motions have $PA_{pm} - PA_j \sim -10^\circ$ to 36° (with an average value $\langle PA_{pm} - PA_j \rangle = 7^\circ$). This decrease in the average angular offset $\langle PA_{pm} - PA_j \rangle$ between the proper motions and the outflow axis shows that there is a partial convergence between the proper motions and the outflow axis as one moves along the HH 110 jet. However, at distances $d > 130''$ from knot A we have knots R and S (see Fig. 3), that again have proper motions that are misaligned with the outflow axis. These proper motions, as stated above, appear to be aligned with the local direction of the curved locus of the jet.

In order to model the HH 270/110 system, Raga et al. (2002) performed 3-D gasdynamics simulations for a radiative jet/cloud collision. Two assumptions for the incident jet velocity were considered: a time-independent, constant direction velocity (*model A*) and a precessing jet of sinusoidally varying velocity (*model B*). In both models, the proper motion velocity vectors deviate from the jet axis direction, and the predicted deviation trend successfully reproduces the observed behaviour in HH 110. Thus, it might be reasonable to interpret the observed lack of symmetry by a jet/cloud collision.

In Fig. 4 we show the magnitude of the proper motion velocities as a function of distance d from knot A. In the $d < 90''$ region, there are 4 low velocity knots (knots B, B′, E and I_E). All of the other knots appear to fall on a general trend of decreasing velocities as a function of d (with knot A having $V_T \simeq 180$ km s^{-1} and knot M, at $d = 81\overset{''}{.}3$, having $V_T \simeq 110$ km s^{-1}). For $d > 90''$, the proper motions of the knots have a wide range of values, from ∼70 km s^{-1} for knot S up to ∼185 km s^{-1} for knot O. Note that for knot O Reipurth et al. (1996) determined a velocity of only 105 km s^{-1}.

Knot B seems have remained nearly stationary through the fifteen years elapsed between the first-epoch and the last-epoch frames, at least within the errors of our proper motion determinations, as shown in Fig. 1 and Table 2. In order to explore the "stationarity" of this region of the jet, we marked as B′ the emission located between knot B and knot C, and we evaluated a proper motion for B′. The proper motion velocity found for B′ is similar to the velocity of knot B. Thus, it appears that HH 110 has a region of a length of ∼14″ along the jet direction (i.e., the region going from the end of knot A to the beginning of knot C) without appreciable proper motions between the first-epoch and last-epoch optical images. The lack of

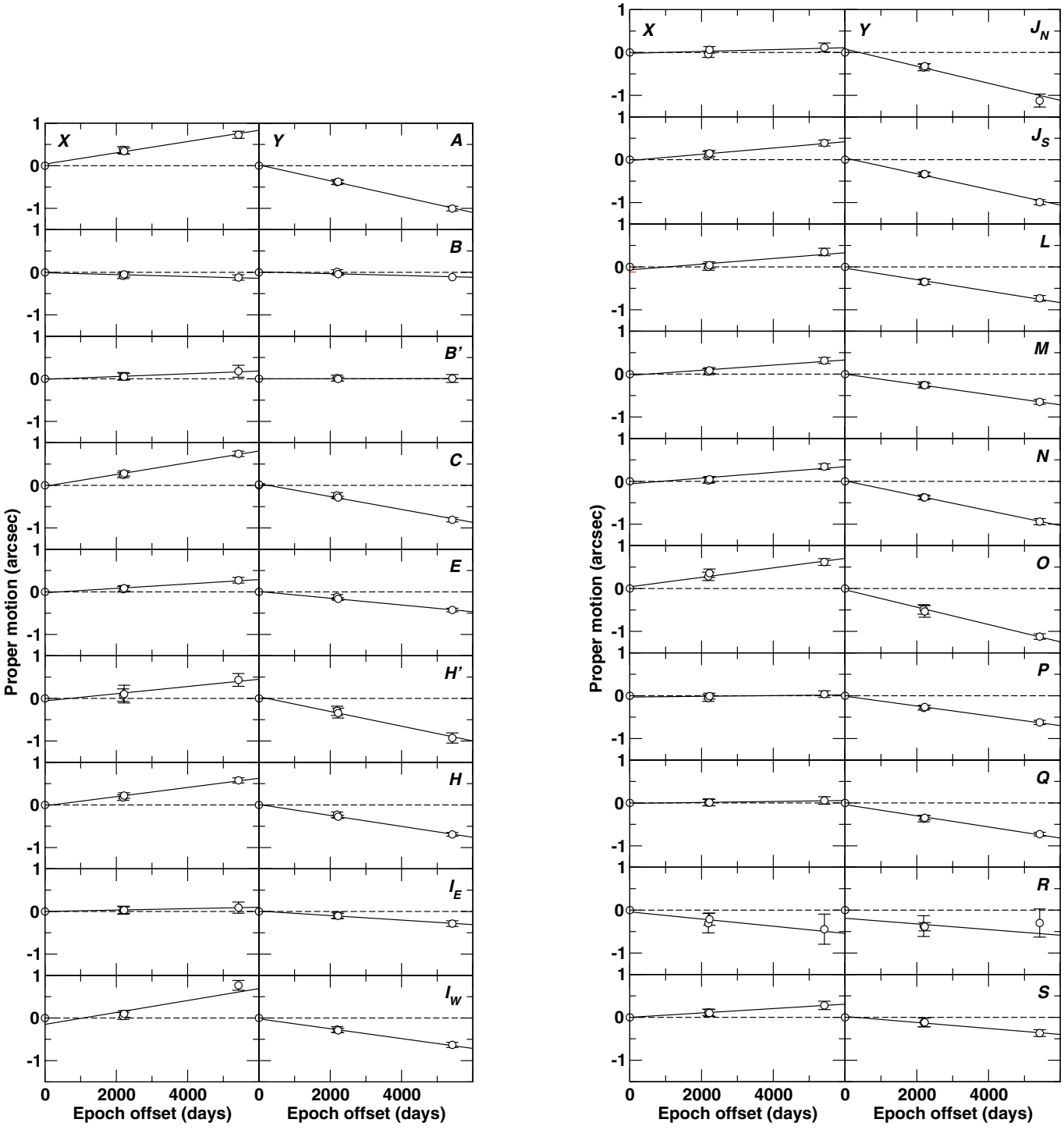

Fig. 2. Proper motions of the HH 110 knots. The offsets in the x direction are shown in the left panels and those in the y direction in the right panels. The knot is indicated in the top right corner of each right panel. For each epoch, a circle represents the displacement (in arcsec) in the x-direction (*left*) and y-direction (*right*) of the corresponding knot, measured from the first-epoch image (which defines the origin of the time scale, set on 1987 Dec. 18). Errors are indicated by the vertical bars. The least squares fits derived for each knot are shown by the continuous lines. The proper motions of the knots in the x, y directions are determined from the slopes of these lines.

motion of knot B is in agreement with the results of Reipurth et al. (1996).

A possible explanation for the nature of the region around knot B is that it might correspond to the location of the jet collision with the cloud. In fact, it should be noted that the values of the [NII]/Hα emission line ratio derived from long-slit spectra around knot B are higher than the values found in its surroundings, around knots A and C (Reipurth et al. 1996; Riera et al. 2003a, Fig. 4). In addition, Riera et al. (2003a) found a minimum in the [SII]/Hα line ratio around knot B relative to its surroundings. This trend in the [NII]/Hα and [SII]/Hα line ratios is indicative of a higher gas excitation around knot B

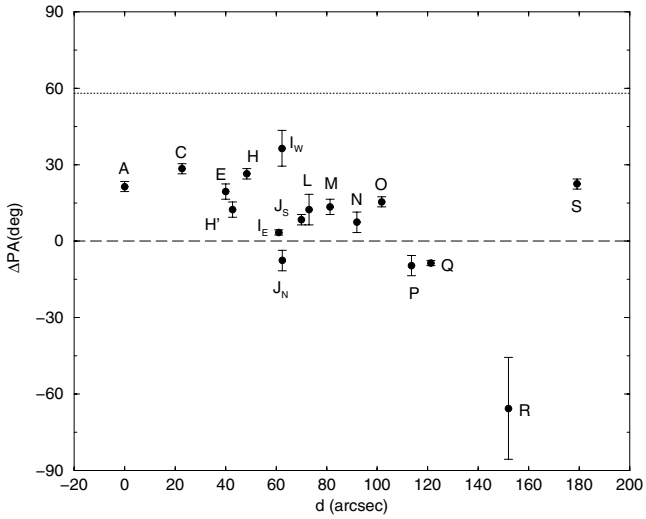

Fig. 3. Deviation of the proper motion velocity direction (PA_{pm}) from the axis of the HH 110 jet (PA_j = 193.°6, reference dashed line) as a function of distance to knot A. The dotted line gives the direction of the axis of HH 270 relative to the HH 110 jet axis. Knots B and B′ are basically stationary (see text) and have been removed from the figure.

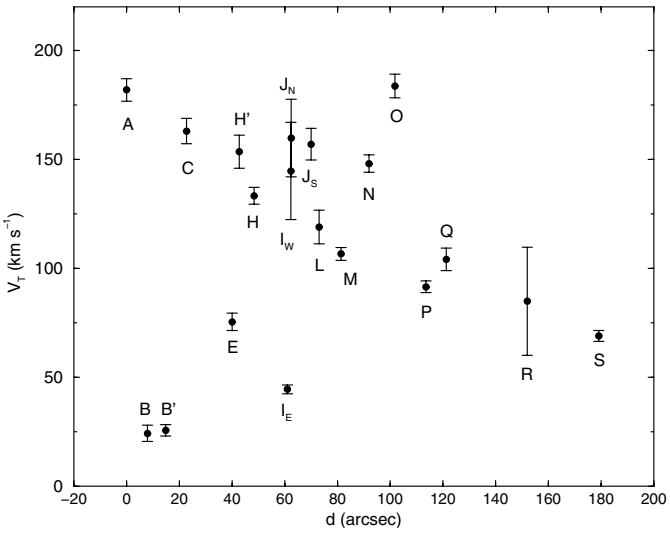

Fig. 4. Moduli of the proper motion velocities of the HH 110 knots, as a function of distance to knot A.

relative to its surroundings and gives support to this interpretation, although alternative explanations are also possible (see next section).

Knot I is elongated in the E-W direction. It has two peaks, which we label I_E and I_W. The ratio of the relative intensities of these two maxima reverses from the 1993 to the 2002 images (with I_E being brighter in 1993 and I_W being brighter in 2002). We find that while I_W shows a proper motion similar to the ones of other nearby knots, I_E shows a much lower proper motion (see Fig. 4). Therefore the proper motion of I_E appears to be somewhat doubtful, and we suspect that it might be the result of a strong change of morphology of the emission in this region, rather than a real motion of a physically well defined knot.

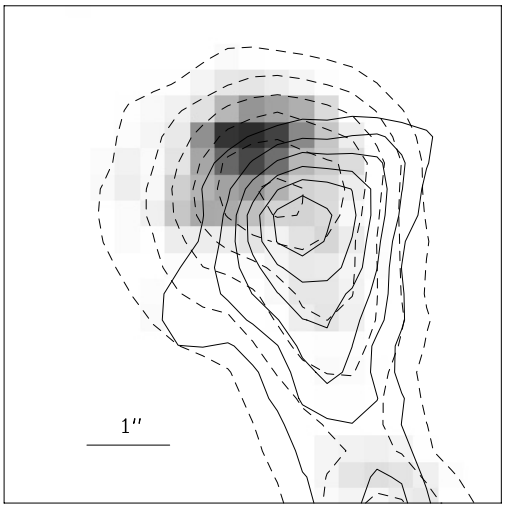

Fig. 5. Close-up of HH 110 knot A from images of Dec. 1987 (grey overlaid), Dec. 1993 (dashed line contours) and Oct. 2002 (solid line contours). North is up and East is to the left.

Finally, for knot A we confirm the change in morphology with time pointed out by Reipurth et al. (1996). In Fig. 5 we show a superposition of the 1987, 1993 and 2002 images of knot A. From this figure we see that the morphology of this region changes quite substantially with time. Not only does the peak of the emission move, but also knot A develops a "tongue" of emitting material extending along the outflow axis. We obtain a proper motion of ∼180 km s^{-1} for knot A, which is higher than the ∼50 km s^{-1} determined by Reipurth et al. (1996). Despite this change in the morphology of knot A, from Fig. 5 it is evident that the peak of knot A shifts as a function of time. This displacement of the peak produces the high proper motion which we find for knot A.

4. Radial and full spatial velocities

From the long-slit spectra obtained along the HH 110 jet axis and across several of its brightest knots, we found that the values of the radial velocity derived from the Hα emission differ by less than 15–20 km s^{-1} (for a spectral resolution of ∼20 km s^{-1}) from the values derived from the [SII] emission (see, e.g., Riera et al. 2003a, Fig. 3). Thus, it seems reasonable to combine proper motions derived from [SII] imaging and radial velocities derived from the Hα emission line to evaluate full spatial velocities of the knots. Accordingly, we used the more complete HH 110 Fabry-Pérot data of the Hα emission line from Riera et al. (2003b) to obtain the heliocentric radial velocity of the HH 110 knots. From these data we computed the line profile integrated over the boxes defined for measuring the proper motions of the knots (see Fig. 1), and determined the radial velocity of the emission peak with a parabolic fit. The results are shown in Fig. 6, where we present the radial velocities with respect to the surrounding cloud (which has a heliocentric radial velocity of +23 km s^{-1}) as a function of distance from knot A.

We can clearly identify two groups of knots in Fig. 6. The first group includes knots A, B, C and E, which show an

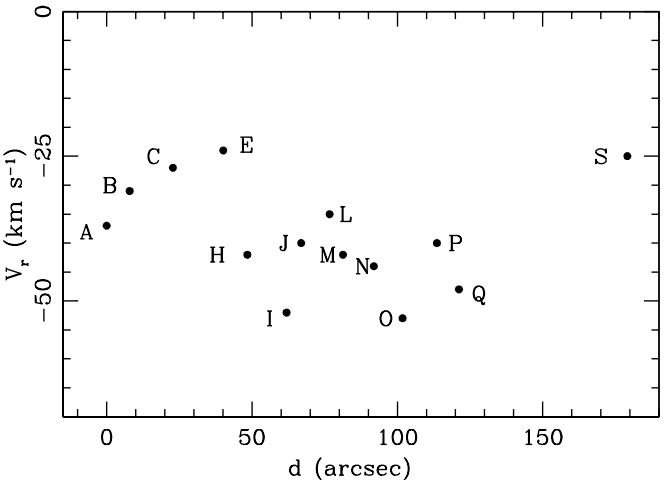

Fig. 6. Radial velocities of HH 110 knots, as a function of distance to knot A. The typical value of the velocity error is ∼10 km s^{-1} .

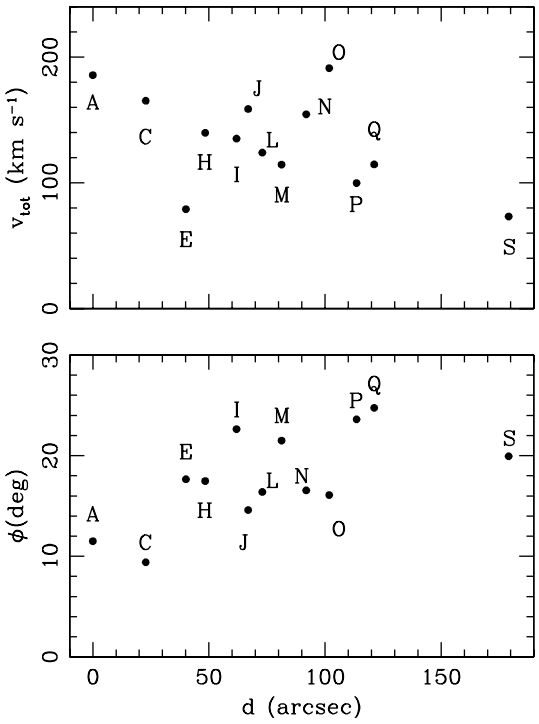

Fig. 7. Total velocities (*upper panel*) and orientation angle, defined by the direction of the knot motion and the plane of the sky (*lower panel*), as a function of distance to knot A. The typical value of the total velocity error is ∼12 km s^{-1}. The typical value of the orientation angle error is ∼6°.

increase of the value of the radial velocity with distance (from ∼−37 km s^{-1} at knot A to ∼−24 km s^{-1} at knot E). The second group corresponds to the knots found at distances from 50″ to 130″ from knot A (including the knots located between knot H and knot Q), which show radial velocities ranging from −38 to −53 km s^{-1}. There is a trend of more negative radial velocities at larger distances, which has been previously reported by Riera et al. (2003a,b). Finally, knot S shows a velocity of ∼−25 km s^{-1} relative to the surrounding cloud.

From the radial velocities (relative to the surrounding cloud, see above and Fig. 6) and the proper motion velocities (see Table 2) we calculated the total spatial velocity $v_{\rm tot}$ of the knots, and the angle ϕ between the knot motion and the plane of the sky (with positive values of ϕ towards the observer). The results of this estimation are shown in Fig. 7. From this figure we see that the orientation angle has a value $\phi = 9°$ to 12° for the region within 30″ from knot A. At larger values of d (>40″), the orientation angle has values $\phi = 15°$ to 25°. This range of ∼10° in orientation angle is consistent with an opening angle of ∼10° (in the plane of the sky) of this region of HH 110 (Riera et al. 2003b).

A general trend of decreasing spatial velocity ($v_{\rm tot}$) with distance (d) can be appreciated from Fig. 7. The velocities decrease from $v_{\rm tot} \simeq 190$ km s^{-1} for knot A to $v_{\rm tot} \simeq 70$ km s^{-1} for knot S. Knots E and O are the ones that show the largest deviations from the general trend of decreasing velocities as a function of distance from knot A.

Regarding knot B, note that the region around this knot is not fully stationary considering the 3-D spatial velocity, since we determined a continuous increase of the radial velocity from knot A to knot C. Thus, instead of being the location of the jet collision with the cloud, an alternative speculative explanation might be that the jet is excavating a channel around knot B, with its entrance around knot A, coming out around knot C.

It should be noted that we carried out the evaluation of the spatial velocity $v_{\rm tot}$ of the knots by assuming that $v_{\rm p}$, the pattern velocity of the knots (i.e., the knot proper motion along the jet axis, $v_{\rm p} = V_{\rm T}/\cos\phi$) is similar to the fluid velocity, $v_{\rm f}$. This condition is fulfilled in the case of highly supersonic, dense jets, where the knots represent internal working surfaces (IWS). However, if the knots originate from Kelvin-Helmholtz (K-H) instabilities, then the ratio $\eta = v_{\rm f}/v_{\rm p}$ could be higher than unity (e.g., up to a factor 2, Micono et al. 1998). If the HH 110 knots originated from K-H instabilities instead of corresponding to IWS, the results we derived give a lower limit to the full spatial velocity $v_{\rm tot}$, and the true jet motion direction ϕ would lie closer to the plane of the sky (i.e., given the low radial velocities found for the HH 110 knots, the values derived for $v_{\rm tot}$ would have to be scaled by a factor of the order of η, while the derived ϕ values would have to be scaled by a factor of the order of η^{-1}). This η scaling value cannot be measured from the present observations, and has to be assumed from a model.

The result we found for the behaviour of the spatial velocity ($v_{\rm tot}$) is very interesting, because it reverses the conclusion of Riera et al. (2003a), who deduced an increasing velocity as a function of distance along the HH 110 flow. The origin of this difference lies in the fact that Riera et al. (2003a) took the measured radial velocities and converted them into a full spatial velocity by deprojecting these radial velocities assuming the same value of $\phi = 35°$ for the orientation angle (with respect to the plane of the sky) for all of the knots. The fact that we now deduce a position-dependent orientation angle for the knots along HH 110 (see Fig. 7) modifies the result of Riera et al. (2003a) in such a way that the observed velocity vs. position trend is now reversed.

The observed trend in the behaviour of the total velocity is not predicted by the jet/cloud models of Raga et al. (2002).

In particular, *model A* gives velocity values significantly lower than the values measured in HH 110 and, in addition, predicts an increase of the proper motion velocity with distance from the cloud (i.e., with the distance from knot A). This prediction is the opposite of the observed trend (i.e., decreasing proper motion velocities away from knot A).

5. Conclusions

We carried out proper motion measurements of the knots of HH 110 on a series of five [SII] 6717+6731 CCD images covering a time baseline of ∼15 years. With these measurements we obtained a better accuracy and were able to describe the motion of more knots than in the previous proper motion determinations of Reipurth et al. (1996). From the Fabry-Pérot data of Riera et al. (2003b), we obtained the average radial velocities for the boxes around the knots that were used for determining the proper motions. Combining these radial velocities with the proper motions, we obtained the full spatial velocities $v_{\rm tot}$ and the orientation angles ϕ (with respect to the plane of the sky) of the different clumps.

We found a number of interesting effects:

- The proper motions of the knots in the northern part of the outflow (i. e., close to knot A) have an orientation angle in between the HH 110 and the HH 270 axes, westward of the HH 110 axis.
- The knots further away from knot A have proper motions which are better aligned with the HH 110 axis.
- The proper motions show a strong lack of symmetry with respect to the outflow axis, and show a general tendency to point towards the west. This trend is predicted by the jet/cloud collision models of Raga et al. (2002).
- There is a region of ∼14″ in length around knot B without appreciable proper motion velocity. We speculate that this region might trace the location of the jet collision with the cloud. Signatures of a higher gas excitation around knot B relative to its surroundings are found from the [NII]/Hα and [SII]/Hα line ratios, which is in favour of this hypothesis, although other explanations are possible.
- Knot R, which is located in a region in which the jet has a highly curved shape, appears to be aligned with the locus of the jet (deviating substantially from the direction of the outflow axis). This result is somewhat marginal, because the proper motion determined for knot R is quite uncertain.
- The spatial velocity $v_{\rm tot}$ shows a general trend of decreasing velocities as a function of distance from knot A (i.e., accounting correctly for the changes in orientation angle, one finds a "deceleration" of the full spatial velocity along the HH 110 flow). This trend in the behaviour of the total velocity is not predicted by the jet/cloud collision models of Raga et al. (2002).

We conclude that HH 110 is a jet with somewhat peculiar characteristics. It should be noted that the spatial velocities of the knots along HH 110 show a decrease by a factor of ∼3 between knot A and knot S. This slowdown occurs over a distance of $\sim 10^{18}$ cm, which is much shorter than the distances over which one expects the braking due to interaction with the surrounding environment to become important (Cabrit & Raga 2002; Masciadri et al. 2002). Therefore, the strong slowdown of the spatial velocity along HH 110 might be an evidence for an anomalously strong interaction between the outflow and the surrounding environment (such as might occur, e.g., during the deflection in a jet/cloud collision). Alternatively, the observed slowdown could be the result of variability in the ejection velocity, or of changes in the jet/cloud impact region. In order to discern between these different possibilities, it will be necessary to carry out further modelling of the HH 270/110 flow.

Acknowledgements. Part of this work was supported by the Spanish MCyT grant AYA2002-00205. The work of ACR was supported by the CONACyT grants 36572-E and 41320 and the DGAPA (UNAM) grant IN 112602. The NOT image was obtained using ALFOSC, which is owned by the Instituto de Astrofísica de Andalucía (IAA) and operated at the NOT under agreement between IAA and the NBIfAFG of the Astronomical Observatory of Copenhagen. We acknowledge Gabriel Gómez (IAC) for obtaining the October 2002 image during the Spanish NOT Service Time. We thank the referee for his/her valuable comments.

References

Cabrit, S., & Raga, A. C. 2002, A&A, 354, 667
Cantó, J., & Raga, A. C. 1996, MNRAS, 280, 559
Cantó, J., Raga, A. C., & Riera, A. 2003, Rev. Mex. Astron. Astrofis., 39, 207
de Gouveia Dal Pino, E. M. 1999, ApJ, 526, 862
Hurka, J. D., Schmid-Burgk, J., & Hardee, P. E. 1999, A&A, 343, 558
López, R., Riera, A., Raga, A. C., et al. 1996, MNRAS, 282, 470
Masciadri, E., de Gouveia Dal Pino, E. M., Raga, A. C., & Noriega-Crespo, A. 2002, ApJ, 580, 950
Micono, M., Massaglia, S., Bodo, G., Rossi, P., & Ferrari, A. 1998, A&A, 333, 1001
Noriega-Crespo, A., Garnavich, P. M., Raga, A. C., Cantó, J., & Böhm, K.-H. 1996, ApJ, 462, 804
Raga, A. C., & Cantó, J. 1995, Rev. Mex. Astron. Astrofis., 31, 51
Raga, A. C., & Cantó, J. 1996, MNRAS, 280, 567
Raga, A. C., de Gouveia Dal Pino, E. M., Noriega-Crespo, A., Mininni, P. D., & Velázquez, P. 2002, A&A, 392, 267
Reipurth, B., & Olberg, M. 1991, A&A, 246, 535
Reipurth, B., Raga, A. C., & Heathcote, S. 1996, A&A, 311, 989
Riera, A., López, R., Raga, A. C., Estalella, R., & Anglada, G. 2003a, A&A, 400, 213
Riera, A., Raga, A. C., Reipurth, B., et al. 2003b, AJ, 126, 327